Shock and Vibration 9 (2002) 105–121
IOS Press

In-situ residual tracking in reduced order modelling

Joseph C. Slater[a,*], Chris L. Pettit[b] and Philip S. Beran[b]
[a]*Wright State University, Dayton, OH 45435, USA*
[b]*Wright-Patterson Air Force Base, OH 45433, USA*

Received 22 August 2001
Revised 17 September 2001

Abstract: Proper orthogonal decomposition (POD) based reduced-order modelling is demonstrated to be a weighted residual technique similar to Galerkin's method. Estimates of weighted residuals of neglected modes are used to determine relative importance of neglected modes to the model. The cumulative effects of neglected modes can be used to estimate error in the reduced order model. Thus, once the snapshots have been obtained under prescribed training conditions, the need to perform full-order simulations for comparison is eliminates. This has the potential to allow the analyst to initiate further training when the reduced modes are no longer sufficient to accurately represent the predominant phenomenon of interest. The response of a fluid moving at Mach 1.2 above a panel to a forced localized oscillation of the panel at and away from the training operating conditions is used to demonstrate the evaluation method.

1. Introduction

Computational determination of flutter boundaries in the transonic regime is an especially demanding problem owing to essential nonlinearities in the aerodynamics. To properly capture the effects of aerodynamic nonlinearities on flutter onset, time-integration methods based on the transonic small-disturbance [6], Euler [15], and Navier-Stokes [7,8,21] equations have been developed to simulate the behavior of aeroelastic systems. Direct methods based on Hopf bifurcation theory also have been developed to compute critical flutter onset speeds of the discrete aeroelastic equations without time integration [3,14]. The former class of techniques generally require large computation times due to the time-accurate nature of the calculations and the large integration times required to establish flow stability properties. The latter class of methods is very efficient for 2-D configurations, but has not been extended to treat 3-D configurations owing to the fully implicit nature of the general procedure.

Recently, Karhunen-Loève (K-L) analysis, or proper orthogonal decomposition (POD), has been used to accelerate greatly the time integration of aeroelastic configurations by reducing system order [9,19]. POD applications to aeroelastic analysis have been limited to time-linearized subsonic and transonic analyses of 2-D configurations. Reduced-order modeling (ROM) with POD is also being applied to unsteady flows for the purpose of developing control models of these systems [16,18]. Other viable ROM strategies proposed and/or tested for aeroelastic analysis and stability prediction include eigenmode techniques [4,5], multiresolution modeling [12] and transition matrix analysis [1]. Pettit and Beran extended POD to a fully nonlinear representation of the discrete Euler equations, and applied the resulting reduced-order model to the simulation of unsteady flow about an oscillating bump [17]. This work followed previous developments of a general framework for studying nonlinear systems with POD, which was tested through the successful reduced-order simulation of limit-cycle oscillation (LCO) onset in a

*Corresponding author: J.C. Slater, Department of Mechanical and Materials Engineering, Wright State University, Dayton, OH 45435, USA. Tel.: +1 937 775 5040; Fax: +1 937 775 5009; E-mail:joseph.slater@wright.edu.

ISSN 1070-9622/02/$8.00

simple system [2]. The current paper extends these results by demonstrating an alternative way to evaluate the importance of selected modes to simulation results in-situ. In-situ monitoring promises to allow the analyst to adjust the ROM during simulation in an appropriate fashion to optimize for simulation speed and accuracy.

2. Galerkin's method applied to a set of 1st order ODEs

Consider a set of nonlinear first order state space equations of the form

$$\dot{\boldsymbol{w}} = \boldsymbol{R}(\boldsymbol{w}; \alpha) \tag{1}$$

where $\boldsymbol{R}$ is a vector of nonlinear functions and α is a parameter, or list of parameters, upon which the system depends. Assume a solution of the form

$$\boldsymbol{w}(t) = \sum_{n=1}^{N} \hat{w}_n(t)\boldsymbol{\phi}_n \tag{2}$$

where $\hat{w}_n(t)$ represent so-called modal coordinates and $\boldsymbol{\phi}_n$ represent so-called mode shapes. This solution form can also be written as

$$\boldsymbol{w}(t) = \Phi\hat{\boldsymbol{w}}(t) \tag{3}$$

where $\Phi = [\boldsymbol{\phi}_1\boldsymbol{\phi}_2\boldsymbol{\phi}_3 \ldots \boldsymbol{\phi}_n]$. Substituting (3) into the equation of motion (1) yields

$$\Phi\dot{\hat{\boldsymbol{w}}} = \boldsymbol{R}(\Phi\hat{\boldsymbol{w}}, \alpha) \tag{4}$$

We define the residual to be

$$\tilde{\mathsf{R}} = \Phi\dot{\hat{\boldsymbol{w}}} - \boldsymbol{R}(\Phi\hat{\boldsymbol{w}}, \alpha) \tag{5}$$

The nth weighted residual is then given by

$$\boldsymbol{\phi}_n^T\tilde{\mathsf{R}} = \boldsymbol{\phi}_n^T\left(\Phi\dot{\hat{\boldsymbol{w}}} - \boldsymbol{R}(\Phi\hat{\boldsymbol{w}}, \alpha)\right) \tag{6}$$

Putting the weighted residuals in vector form, and constraining them to be equal to zero yields

$$\Phi^T\tilde{\mathsf{R}} = \Phi^T\left(\Phi\dot{\hat{\boldsymbol{w}}} - \boldsymbol{R}(\Phi\hat{\boldsymbol{w}}, \alpha)\right) = \boldsymbol{0} \tag{7}$$

Solving for $\dot{\hat{\boldsymbol{w}}}$ yields the reduced-order equations of motion as

$$\dot{\hat{\boldsymbol{w}}} = \left(\Phi^T\Phi\right)^{-1}\Phi^T\boldsymbol{R}(\Phi\hat{\boldsymbol{w}}, \alpha) \tag{8}$$

which can be simulated in time, using larger time steps [2,17,13] than the original equations of motion, with the intention of obtaining results functionally equivalent to those that would have been obtained from a full-order model simulation.

3. Karhunen-Loève analysis

The mode vectors, $\boldsymbol{\phi}_m = 1, 2, 3, \ldots, n$, can be, and often are, obtained using Karhunen-Lo ève analysis (also referred to as proper orthogonal decomposition, or POD) [11,19]. A set of snapshot vectors, $\boldsymbol{w}^{(i)}$, are generally obtained through integration of the full system Eq. (1) for some predefined conditions similar to the current analysis. Choice of the predefined conditions is based upon "average" operating conditions. The hope is that the space covered by the training simulation is sufficient to cover the space within which the second simulation, the reduced-order simulation, should operate. If not, then a full-order simulation can/should be performed under the perturbed operating conditions in order to generate snapshots more useful over the new local domain.The vectors are combined into a snapshot matrix $S = \left[\boldsymbol{w}^{(1)}\boldsymbol{w}^{(2)}\boldsymbol{w}^{(3)} \ldots \boldsymbol{w}^{(i)}\right]$. A reduced set of vectors, Φ, are obtained from these snapshots representing the space spanned by S in an optimal fashion. Considering the term $\left(\Phi^T\Phi\right)$ in Eq. (8). Substituting $\Phi = SV$ yields

$$\left(\Phi^T\Phi\right) = V^TS^TSV \tag{9}$$

If the matrices V are chosen to be the eigenvectors of S^TS, then

$$\left(\Phi^T\Phi\right) = V^TS^TSV = \Lambda \tag{10}$$

where Λ is the diagonal eigenvalue matrix of S^TS. Since V is orthonormal, $V^T = V^{-1}$. Thus, the solution of the eigenvalue problem

$$S^TSV = V\Lambda \tag{11}$$

along with the relation $\Phi = SV$ yields a set of orthogonal modes Φ. The magnitude of each of the eigenvalues Λ represents the degree to which the corresponding eigenvector, $\boldsymbol{v}_i$, participates in the set of snapshots. As a result of this analysis, the modes are weighted by the square root of the eigenvalues λ. Modes that do not participate "significantly" in the snapshots are truncated. The more commonly used form of the reduced-order equations is obtained by substituting $\Phi = SV$ and Eq. (10) into Eq. (8) yielding

$$\dot{\hat{\boldsymbol{w}}} = (\Lambda)^{-1}V^TS\boldsymbol{R}(\Phi\hat{\boldsymbol{w}}, \alpha) \tag{12}$$

The shortcoming of this approach is that there is no guarantee that the mode shapes obtained from one simulation will be sufficient to span the space of another simulation. When performing the reduced-order simulation, it becomes necessary to truncate the vectors Φ to only those containing sufficient energy content

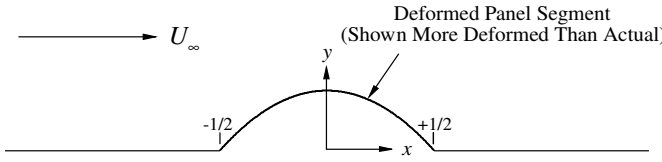

Fig. 1. Schematic of panel and coordinate system.

(significant eigenvalues, λ) [17] or else Eq. (12) can break down due to the near singularity of the matrix Λ. Likewise, Eq. (10) illustrates that the sensitivity exists even when using the formulation of Eq. (8). Thus an "optimal" truncation method is necessary.

An alternative formulation is possible by unweighting the mode shapes $\boldsymbol{\phi}$ by dividing them each by the square root of their corresponding eigenvalues. Thus the eigenvalue problem described by Eq. (10) becomes

$$\begin{aligned}\Lambda^{-\frac{1}{2}}\Phi^T\Phi\Lambda^{-\frac{1}{2}} &= \bar{\Phi}^T\bar{\Phi} \\ &= \Lambda^{-\frac{1}{2}}V^TS^TSV\Lambda^{-\frac{1}{2}} = I\end{aligned} \tag{13}$$

The advantage of this formulation is that the equation of motion Eq. (8) can be simplified to the form

$$\dot{\hat{\boldsymbol{w}}} = \bar{\Phi}^T\boldsymbol{R}(\bar{\Phi}\hat{\boldsymbol{w}}, \alpha) \tag{14}$$

where $\bar{\Phi}$ represent the unit length mode shapes. The elements of the eigenvalue matrix Λ can have a variation of multiple orders of magnitude. There is some concern that this may impact stability and/or accuracy of the simulations as a result of roundoff error, however this hypothesis has not yet been tested.

4. Validation of simulation results

The weighted residual is given in Eq. (6) as

$$\bar{\boldsymbol{\phi}}_n^T\tilde{\mathsf{R}} = \bar{\boldsymbol{\phi}}_n^T\left(\bar{\Phi}\dot{\hat{\boldsymbol{w}}} - \boldsymbol{R}(\bar{\Phi}\hat{\boldsymbol{w}}, \alpha)\right) \tag{15}$$

Recall that for n greater than some chosen value, N, this weighted residual is not constrained to be zero because some of the modes $\boldsymbol{\phi}_n$ were truncated in the reduced-order analysis. From Eq. (10) it can be seen that for any n greater than N, $\boldsymbol{\phi}_n^T\Phi = \mathbf{0}$ due to the orthogonality of the modes. The second part of the residual is not necessarily zero and thus the weighted residual for $n > N$ is given by

$$\bar{\boldsymbol{\phi}}_n^T\tilde{\mathsf{R}} = \bar{\boldsymbol{\phi}}_n^T\left(-\boldsymbol{R}(\bar{\Phi}\hat{\boldsymbol{w}}, \alpha)\right) \tag{16}$$

It is a reasonable assumption that these truncated modes become more significant for simulations in adjacent regions of the design space (e.g. $\alpha \neq \alpha_0$). Thus the magnitude of the ignored weighted residuals, given by Eq. (16), can be monitored during simulation. A significant increase in the values as compared to their nominal values obtained during training can be used as an indicator of error in the reduced-order simulation.

5. Test problem

The ROM/POD framework described above for analyzing unsteady solution behavior is placed in a program called RAPOD, which is designed to be problem independent, except for evaluation of the full-system array, $\boldsymbol{R}$ [17]. To test the RAPOD implementation for the unsteady response of a flowfield to time-dependent changes in geometry, we have studied the problem of inviscid flow over a 2-D, oscillating bump using the Euler equations.

The flowfield is assumed to occur above an infinite, segmented panel that nominally lies in the $y = 0$ coordinate plane, and whose surface is defined by $y_s(x,t)$ (see Fig. 1). A deforming segment of the panel is specified between $x = -1/2$ and $x = 1/2$ such that the segment length, c, is normalized to unit value. Away from the deforming segment, the panel is flat ($y_s(x,t) = 0$, $|x| > 1/2$), while over the deforming segment, a time-dependent deflection is specified:

$$\delta(t) = \delta_1\cos(\omega t)\left(1 - e^{-\beta t}\right), \tag{17}$$

$$y_s(x,t) = \delta\left(1 - 4x^2\right) \qquad (|x| \leqslant 1/2), \tag{18}$$

where δ_1 is a deflection amplitude, ω is a frequency, and β is a modulation parameter to adjust the short-time behavior of the system. The spatial and temporal variables are non-dimensionalized using c and the aerodynamic characteristic time based on the far-field velocity U_∞. The instantaneous shape of the panel is that of a parabolic arc with maximum deflection $|\delta(t)|$ at $x = 0$. The large-time behavior of $\delta(t)$ is $\delta_1\cos(\omega t)$, which represents simple periodic motion of the bump height.

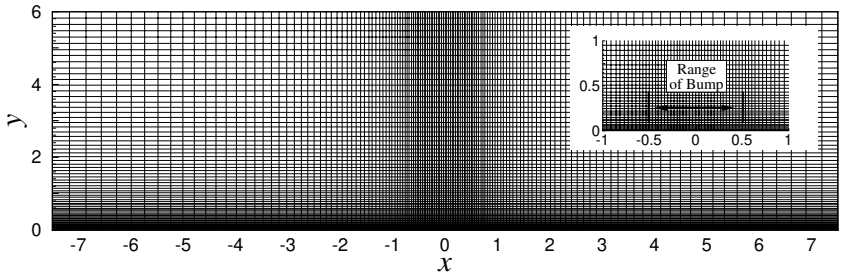

Fig. 2. Baseline grid.

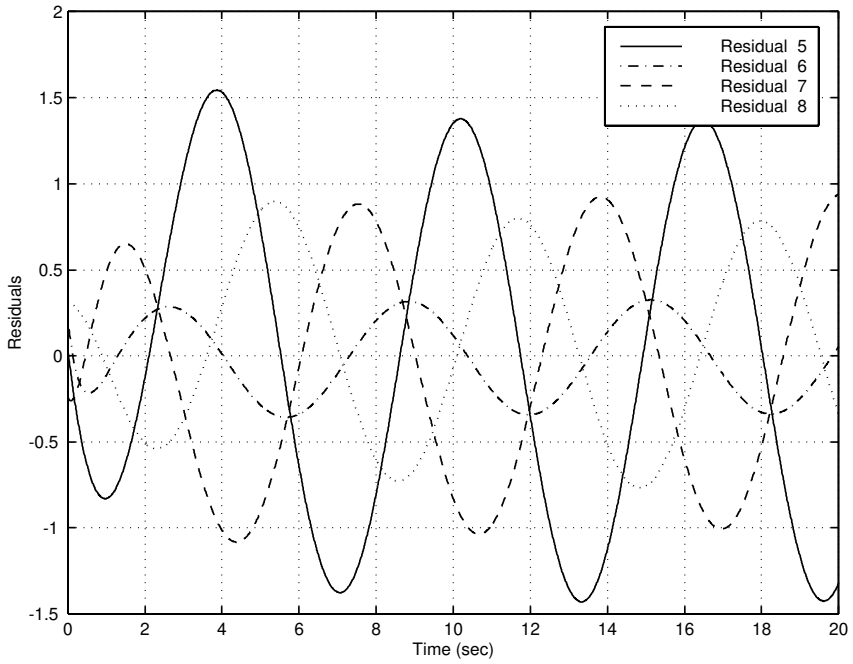

Fig. 3. Residuals 5–8 for 4 mode simulation with $\delta_1 = 0.005$.

6. Initial and boundary conditions

Initially, the flow is that of the freestream state and the panel is undeflected. After using the scales defined above and non-dimensionalizing density by the far-field value, ρ_∞, and pressure by $\rho_\infty U_\infty^2$, the non-dimensional farfield conditions are

$$\begin{aligned} &\rho \to 1, \quad u \to 1, \quad v \to 0, \\ &p \to 1/(\gamma M_\infty^2), \end{aligned} \tag{19}$$

where p is the pressure, (u, v) are velocity components in the (x, y) coordinate directions, γ is the ratio of specific heats, and M_∞ is the freestream Mach number.

In a conventional simulation of the aerodynamic response to an oscillating bump, a deforming, panel-conforming grid would be used in the discretization of the flowfield. To avoid potential difficulties associated with grid deformation and the reduced-order modeling procedure described above, a transpiration boundary condition is applied at $y = 0$ to model the effects of a moving boundary [20]. For the bump problem examined herein, the transpiration boundary condition involves the enforcement of the exact condition of impermeability at the panel surface,

$$-u\frac{\partial y_s}{\partial x} + v = \frac{\partial y_s}{\partial t} \qquad (y = y_s(x,t)), \tag{20}$$

at $y = 0$. This transfer of boundary conditions is identical to that employed in small-disturbance theory, and assumes regularity of the computed solution and smallness of the deformation: $y_s(x,t) \ll 1$. In addition to impermeability, we apply additional conditions to close the discretized Euler equations at the panel surface:

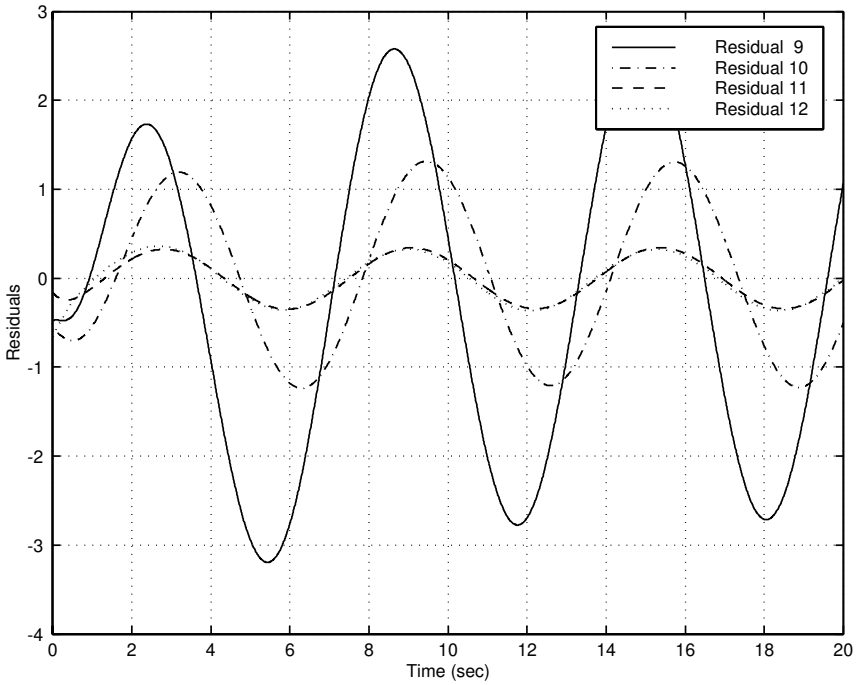

Fig. 4. Residuals 9–12 for 4 mode simulation with $\delta_1 = 0.005$.

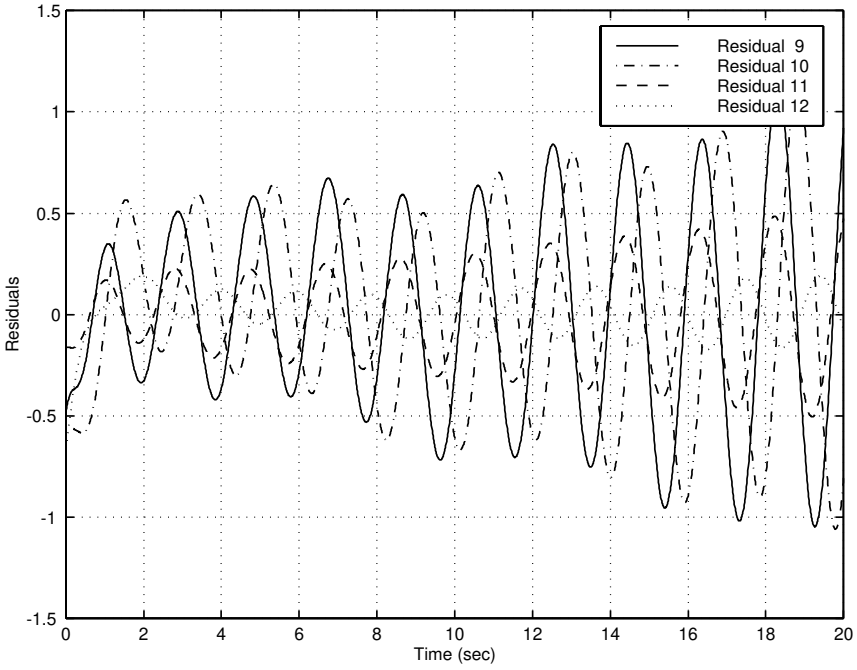

Fig. 5. Residuals 9–12 for 8 mode simulation with $\delta_1 = 0.005$.

$$\frac{\partial u}{\partial y} = \frac{\partial p}{\partial y} = \frac{\partial \rho}{\partial y} = 0 \qquad (y = 0) \tag{21}$$

In Eq. (21), derivatives of primitive variables with respect to the y-coordinate are specified to vanish, rather than the coordinate normal to the deformed panel. This approximation assumes smallness of deforma-

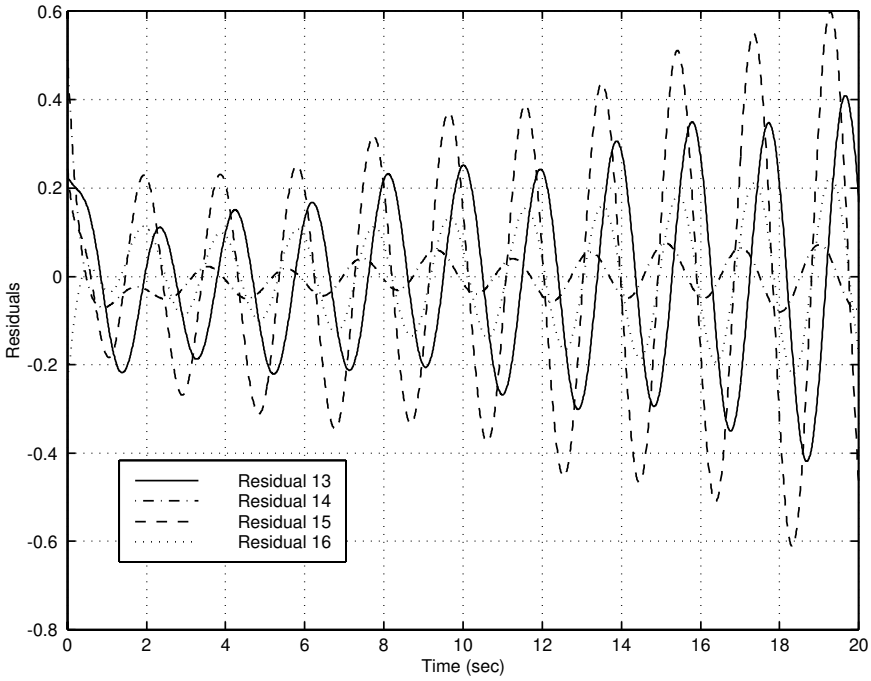

Fig. 6. Residuals 13–16 for 8 mode simulation with $\delta_1 = 0.005$.

tion slopes, consistent with the prior assumption of $y_s(x,t) \ll 1$.

7. Grid construction

The flow is simulated over a physical domain of length L, centered about $x = 0$ and height H. The domain is discretized using I nodes in the streamwise direction and J nodes normal to the panel. Indices i ($1 \leqslant i \leqslant I$) and j ($1 \leqslant j \leqslant J$) are used to denote grid points at which variables are evaluated. Grid points corresponding to $j = 1$ are placed on the x-coordinate line and do not move with changes in δ. Grid points are clustered in the direction normal to the panel at the panel surface, with the minimum spacing denoted by Δ_{wall}. The spacing of grid points is specified to grow geometrically with normal index position from the panel boundary. In the streamwise direction, the node spacing is chosen to be uniform over the deforming panel segment, while growing geometrically upstream of the leading edge (positioned at $i = I_{LE}$) and downstream of the trailing edge (positioned at $i = i_{TE}$). A baseline grid, shown in Fig. 2, is constructed with the following values: $I = 141$, $J = 71$, $L = 15$, $H = 6$, $I_{LE} = 55$ and $I_{TE} = 85$. For the baseline grid, $\Delta_{\text{wall}} \approx 0.0137$.

8. Governing equations and method of solution

The governing aerodynamic equations are the Euler equations, cast in nondimensional form for a general curvilinear coordinate system (ξ,η). For the grid described above, the ξ coordinate runs in the x-coordinate direction, whereas η is associated with the y coordinate. The equations are expressed in terms of conserved variables, $U \equiv [\rho, \rho u, \rho v, E_t]^T$:

$$\frac{\partial \hat{U}}{\partial t} + \frac{\partial \hat{E}(U)}{\partial \xi} + \frac{\partial \hat{F}(U)}{\partial \eta} = 0, \tag{22}$$

where $\hat{U} = U/(\xi_x \eta_y - \xi_y \eta_x)$, and $\hat{E}$ and $\hat{F}$ are transformed flux arrays [14]. The aerodynamic equations are placed in discrete form following the upwind total variation diminishing (TVD) scheme of Harten-Yee [10,23], with a correction for grid-point motion. The discretization of second-order or first-order spatial accuracy, depending on parameter selection, and first-order temporal accuracy is expressed as [3]

$$\begin{aligned} \frac{\hat{U}^{n+1}_{i,j} - \hat{U}^{n}_{i,j}}{\Delta_t} = {} & \tilde{\hat{F}}^{n}_{i,j-\frac{1}{2}} - \tilde{\hat{F}}^{n}_{i,j+\frac{1}{2}} \\ & + \tilde{\hat{E}}^{n}_{i-\frac{1}{2},j} - \tilde{\hat{E}}^{n}_{i+\frac{1}{2},j}, \end{aligned} \tag{23}$$

where the arrays $\tilde{\hat{E}}$ and $\tilde{\hat{F}}$ are modified numerical fluxes

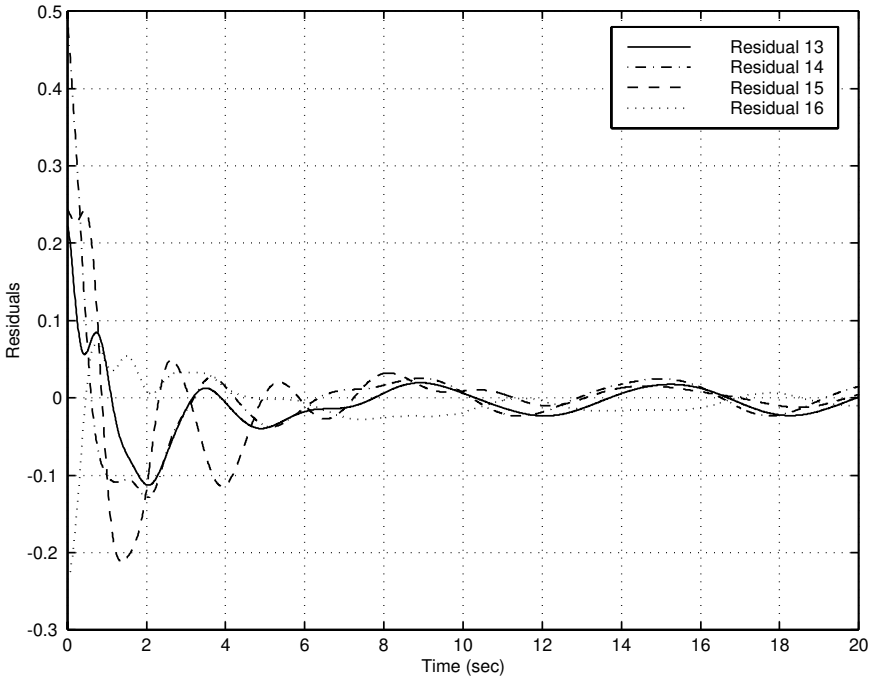

Fig. 7. Residuals 13–16 for 12 mode simulation with $\delta_1 = 0.005$.

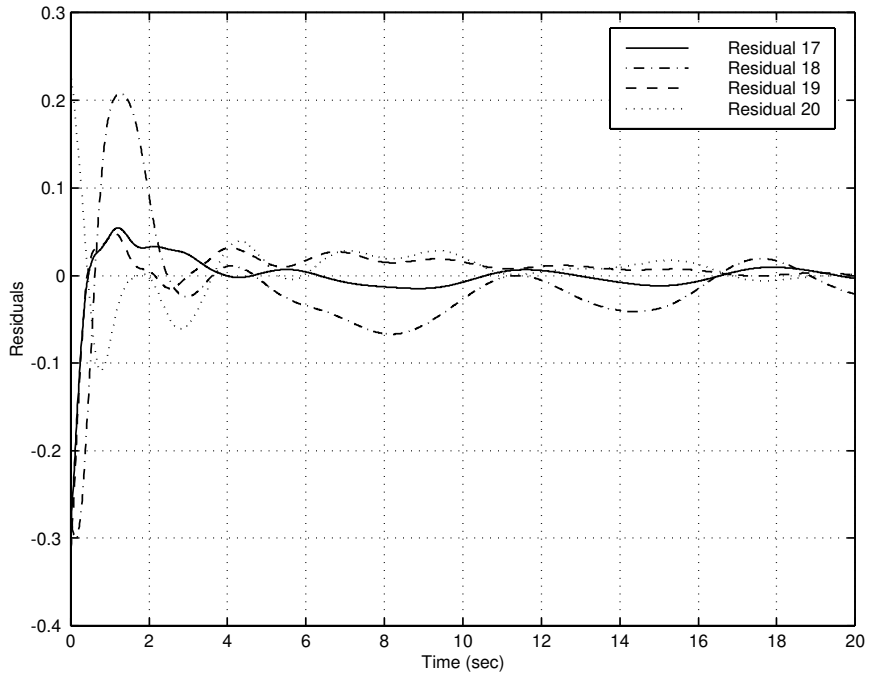

Fig. 8. Residuals 17-20 for 12 mode simulation with $\delta_1 = 0.005$.

that implement the TVD formulation.

Conditions for boundary nodes, except on the panel surface ($y = 0$), are developed and placed in first-order evolutionary form to be consistent with Eq. (1). Freestream conditions are enforced along the inflow and farfield boundary ($y = H$) using the soft evolu-

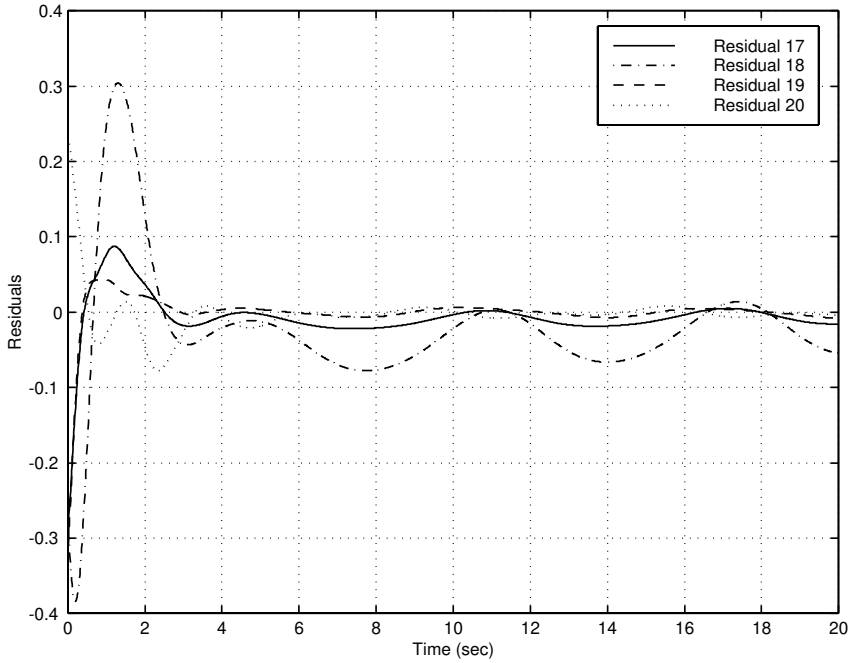

Fig. 9. Residuals 17–20 for 16 mode simulation with $\delta_1 = 0.005$.

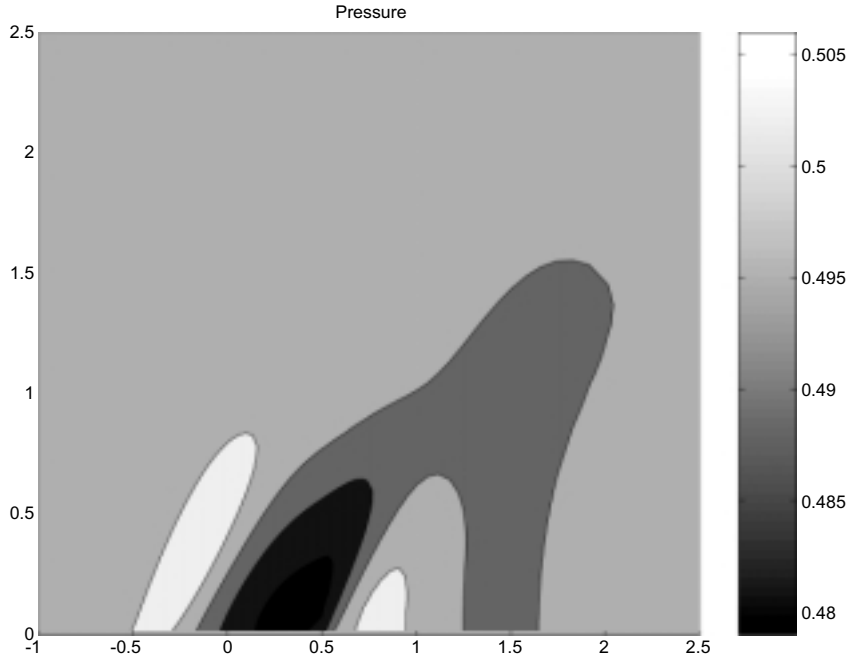

Fig. 10. Pressures after 20 second simulation using 8 modes with $\delta_1 = 0.005$.

tionary equation $(q^{n+1} - q^n)/\Delta_t = -(q^n - q_\infty)/\Delta_t$, where q is a conserved variable. Outflow conditions are similarly enforced with a convective equation: $(q^{n+1} - q^n)/\Delta_t = -u(\xi_x q^n_\xi + \eta_x q^n_\eta)$.

9. Results

This section describes sample results from the oscillating bump problem for $M_\infty = 1.2$ and $\gamma = 1.4$.

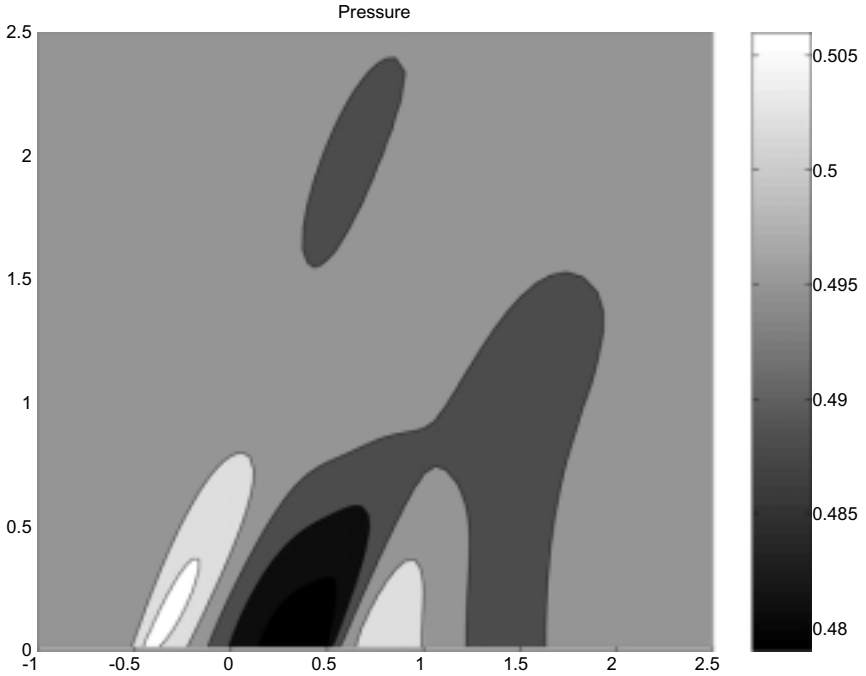

Fig. 11. Pressures after 20 second simulation using 12 modes with $\delta_1 = 0.005$.

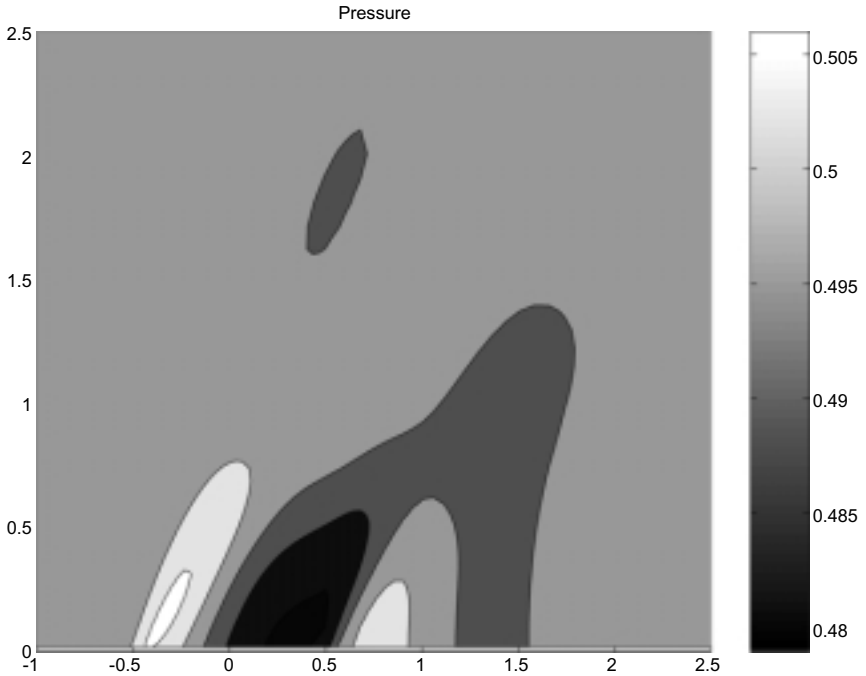

Fig. 12. Pressures after 20 second simulation using 16 modes with $\delta_1 = 0.005$.

Snapshots were collected by integrating the full system with $\Delta t = 0.01$, $\delta_1 = 0.005$, $\omega = 1.0$, and $\alpha = 3.0$. Two thousand iterations were performed using first-order spatial accuracy and snapshots were taken every 25 iterations for a total of 80 snapshots. Although the RAPOD algorithm was constructed to permit taking

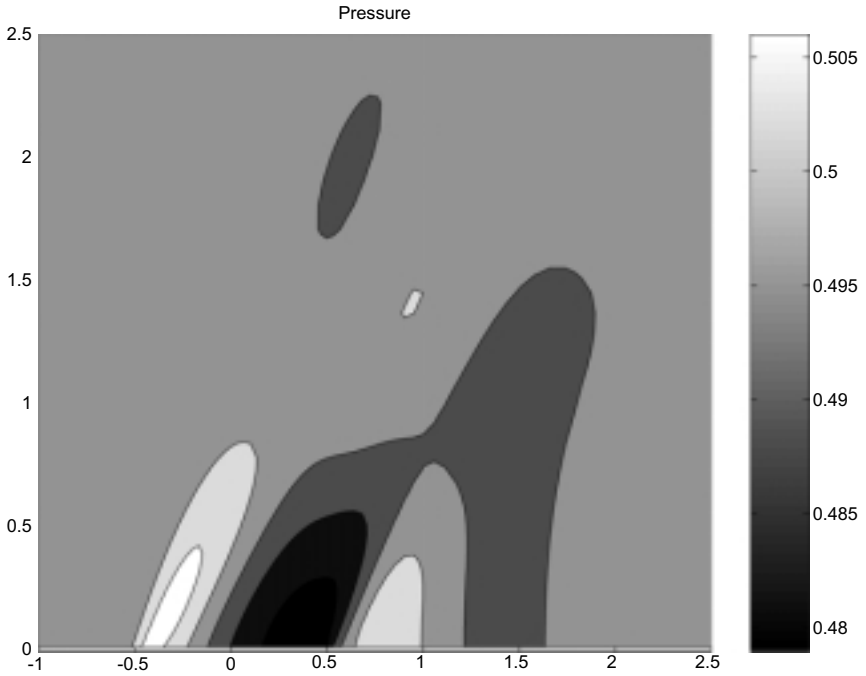

Fig. 13. Pressures after 20 second simulation, full model with $\delta_1 = 0.005$.

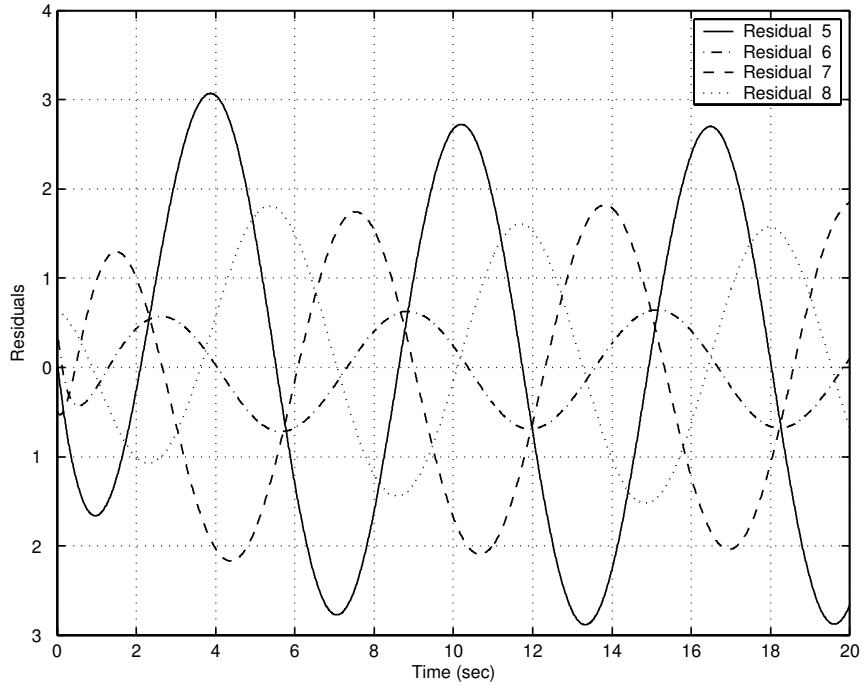

Fig. 14. Residuals 5-8 for 4 mode simulation with $\delta_1 = 0.01$.

snapshots at a response-dependent rate, this capability was not used in the present problem.

Modes were generated as described by Eqs (9–14) and ranked, in the traditional manner, by decreasing eigenvalue. The first 24 modes were kept for the analyses, and four reduced-order model simulations were

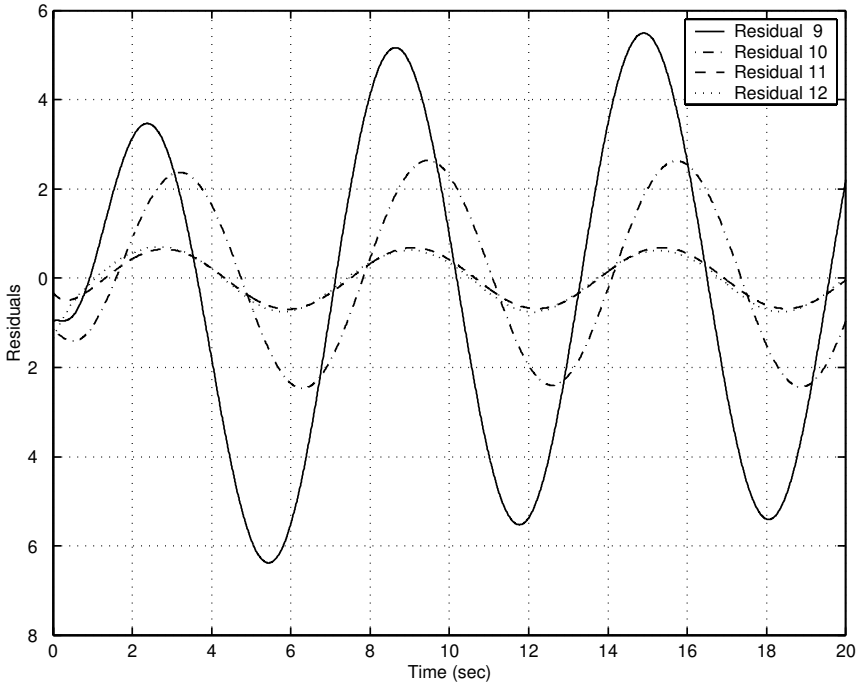

Fig. 15. Residuals 9–12 for 4 mode simulation with $\delta_1 = 0.01$.

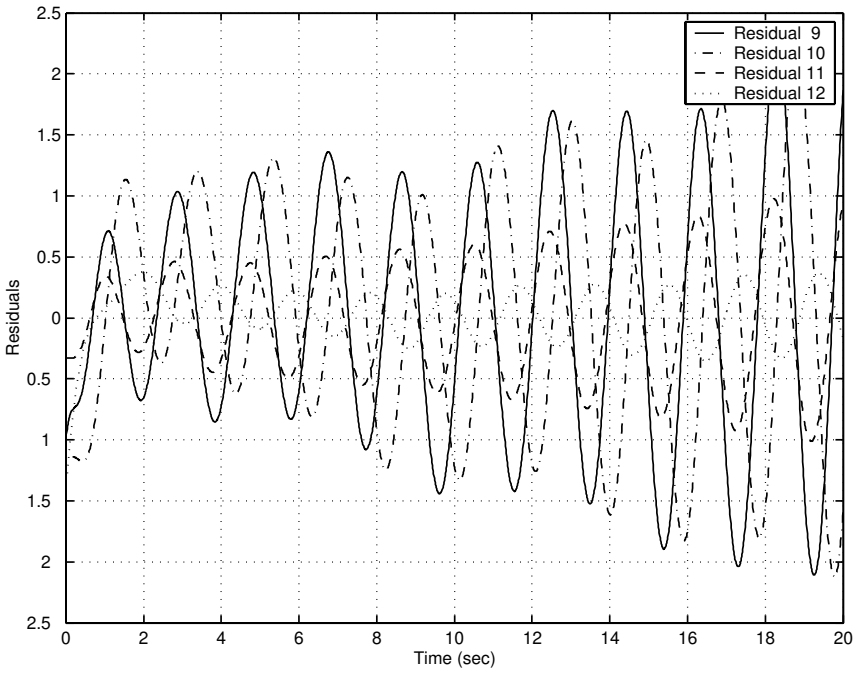

Fig. 16. Residuals 9–12 for 8 mode simulation with $\delta_1 = 0.01$.

performed: one each using the first 4, 8, 12, and 16 modes. In addition, simulations were repeated for the off-training-condition of $\delta_1 = 0.01$.

For the 4 mode reduced-order simulation, observing Fig. 3 in the fully developed part of the solution, the residuals decrease in the order of modes 5, 7, 8, then

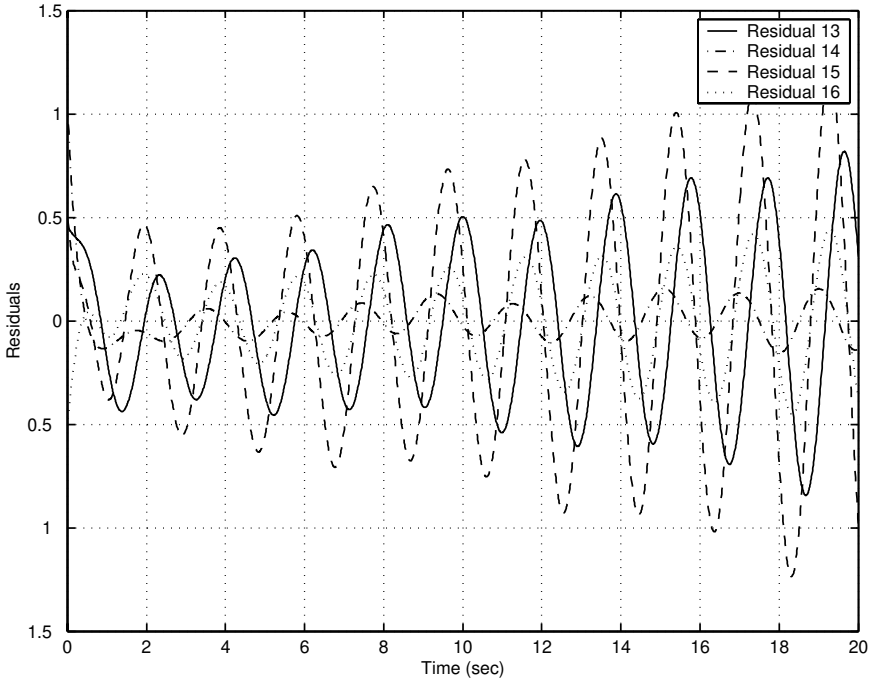

Fig. 17. Residuals 13-16 for 8 mode simulation with $\delta_1 = 0.01$.

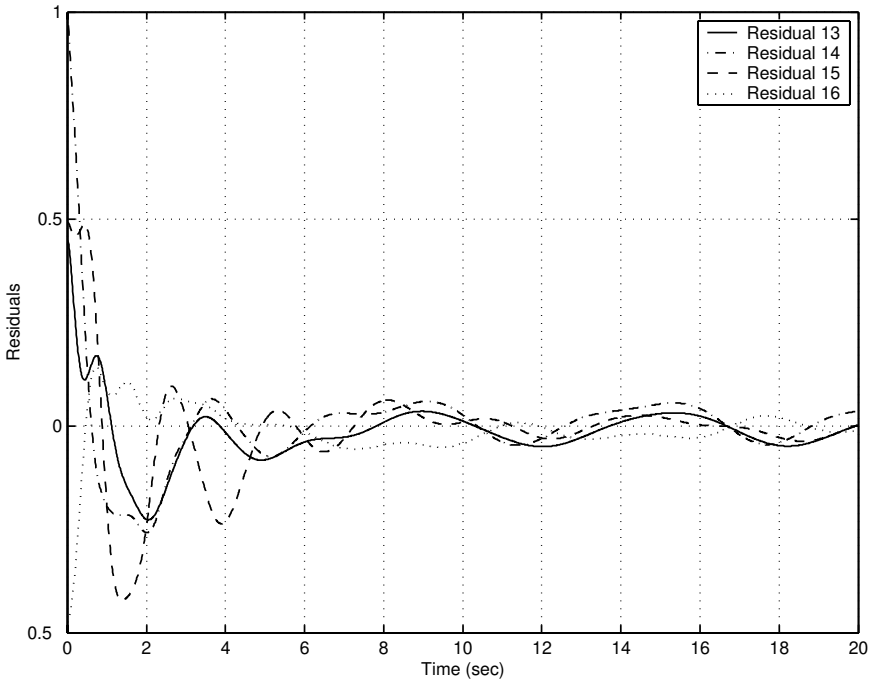

Fig. 18. Residuals 13–16 for 12 mode simulation with $\delta_1 = 0.01$.

6, while Fig. 4 shows that two of the later modes have greater residuals than that for mode 5. This seems to indicate that choosing to perform the simulation with 8 modes would result in significant error as compared to the full order solution.

Performing an 8 mode simulation results in residuals

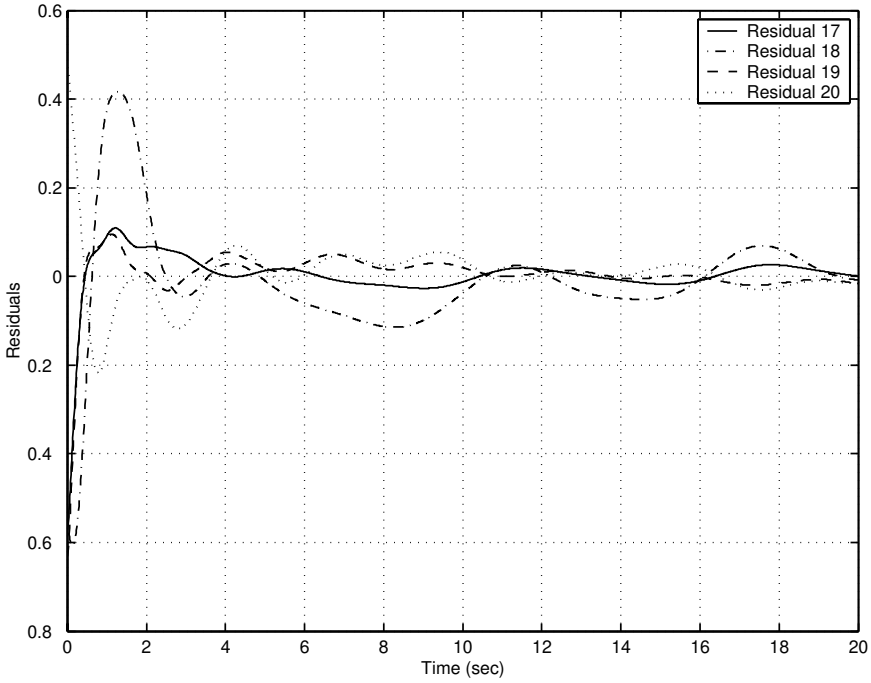

Fig. 19. Residuals 17–20 for 12 mode simulation with $\delta_1 = 0.01$.

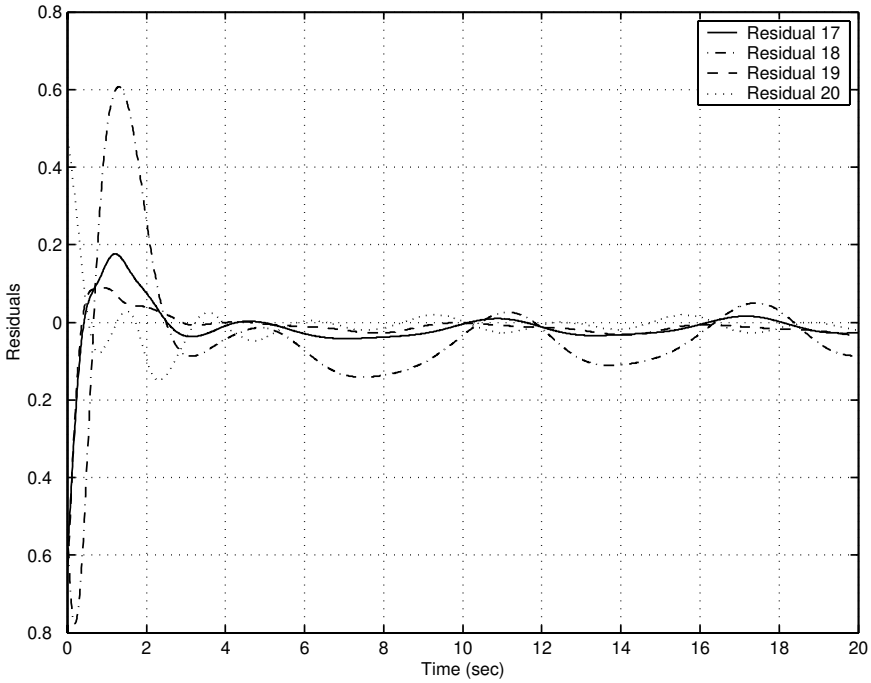

Fig. 20. Residuals 17–20 for 16 mode simulation with $\delta_1 = 0.01$.

for the higher modes that are increasing with time (See Figs 5 and 6). It is not possible from the simulation to determine whether the simulation is unstable, or if at some point the error will be self limiting. Instability of reduced-order models has been observed by the authors for other systems. The phenomenon is not yet widely

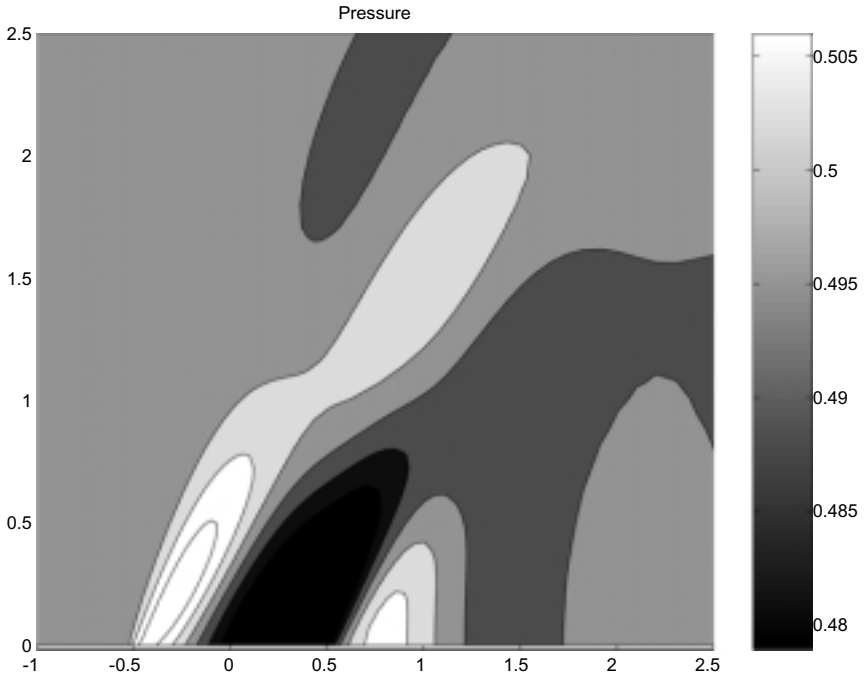

Fig. 21. Pressures after 20 second simulation using 8 modes with $\delta_1 = 0.01$.

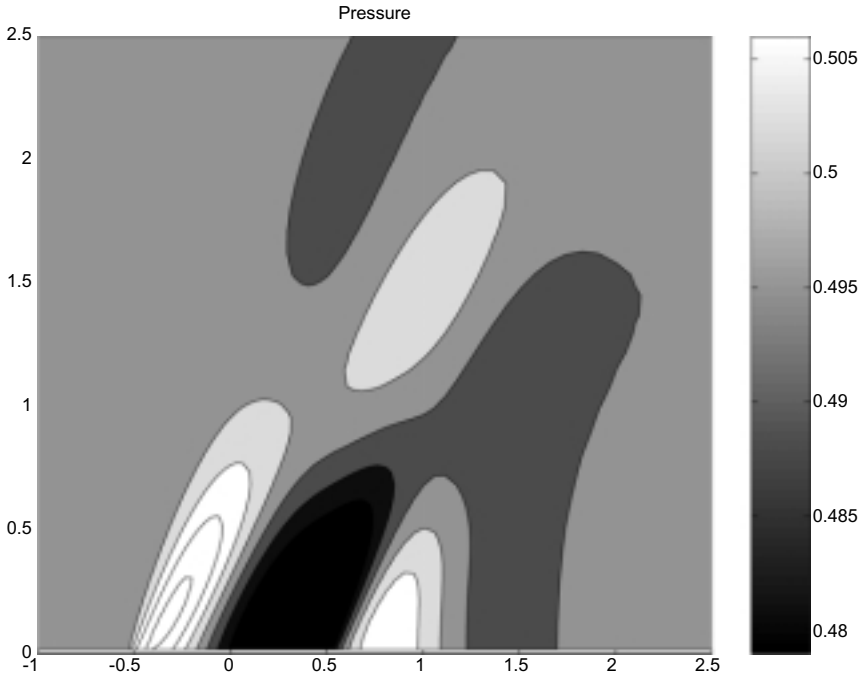

Fig. 22. Pressures after 20 second simulation using 12 modes with $\delta_1 = 0.01$.

understood, and is currently under investigation. A simple example illustrating this phenomenon is given by Slater [22]. On the contrary, the 12 mode simulation (Figs 7 and 8) shows residuals that tend to remain small over time, and are remaining well below 0.1, with the exception of mode 18 which approaches 0.1 in the late

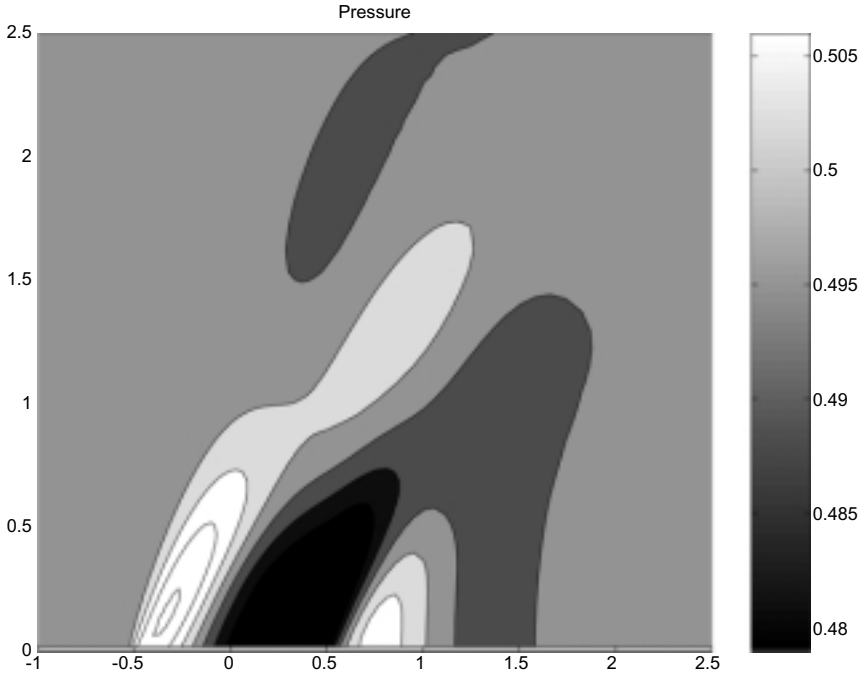

Fig. 23. Pressures after 20 second simulation using 16 modes with $\delta_1 = 0.01$.

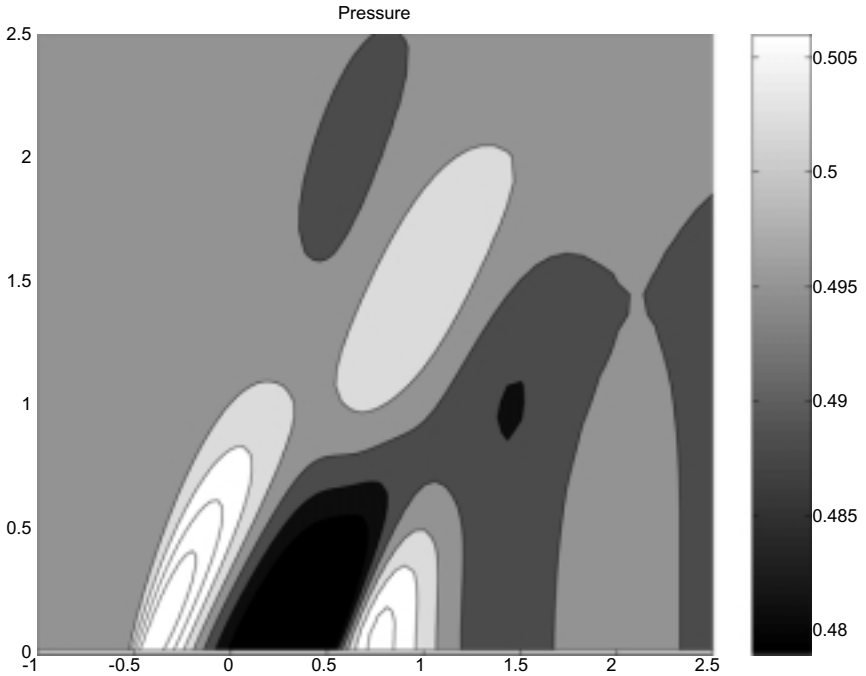

Fig. 24. Pressures after 20 second simulation, full model with $\delta_1 = 0.01$.

transient part of the response.

The 16 mode simulation (Fig. 9) shows results similar to the 12 mode simulation. The only mode of concern is mode 18, which has a greater residual than all other modes 13–20 for both the 12 and 16 mode models. However, when compared to the 4 and 8 mode simula-

tions, it is clear that including additional modes in the reduced order model will have a relatively negligible effect.

One could conclude that 12 modes are sufficient by referring to Figs 7 and 8. In fact, referring to Figs 10–13, it is apparent that very little improvement in the model is made by including modes 13 or higher.

The results shown in Figs 7 and 8 suggest that 12 retained modes are sufficient to capture accurately the aerodynamic response to bump oscillation. This observation is reinforced through comparison of pressure fields computed with 8-, 12- and 16-mode ROMs at $t = 20$ (shown in Figs 10–12). In each of these contour plots, pressure values are in close agreement with results computed using the full-system equations, reproducing flow structure adjacent to, and away from, the oscillating bump. In addition, Figs 7–9 illustrate that the higher modes are important only for representing the startup transient. This trait was previously noted by Pettit and Beran [17]. However, Fig. 8 also illustrates that mode 18 contributes to the response when the flow is fully developed.

Figures 14–24 repeat Figs 3–13 for $\delta_1 = 0.01$. In comparing equivalent figures for the two values of δ_1, one observes that the effect of doubling the perturbation amplitude is to double the residual error. This is not altogether surprising, as the linear terms of the governing equations are dominant for these results. However, some measure of the degree of nonlinearity can be observed by noting deviations from the linear assumption, which are minimal in this case. A reasonable conclusion can then be made that the modes used for a perturbation of $\delta_1 = 0.005$ are equally as valid for a perturbation of $\delta_1 = 0.01$. Comparing the differences between Figs 12 and 13 (18 modes versus full order model for $\delta_1 = 0.005$) to the differences between Figures (23) and (24) (18 modes versus full order model for $\delta_1 = 0.01$) one notes that the reduced order models are of the same relative quality, thus validating the use of residual estimates to evaluate reduced order model simulation quality.

10. Conclusions

A method has been introduced for in-situ evaluation of reduced-order modeling. The *importance* of modes can be measured differently than has been done in the previous work. Here it is proposed that the magnitude of truncated residuals be used as a measure of lost information. This is as opposed to the often-used energy content (eigenvalue) ranking of the modes based on a training simulation under potentially different operating conditions or different regimes of operation (e.g. start-up or fully developed). Hence the importance of a mode can be evaluated more appropriately for the current simulation, enabling a more appropriate selection of a set of modes in the reduced-order simulation.

Acknowledgements

The first author would like to thank the Air Force Research Laboratory for support through the Air Vehicles Directorate Summer Faculty Research Program (Dr. Beran, Research Manager).

References

[1] O. Bauchau and Y. Nikishkov, Aeroelastic Stability Analysis using Reduced Order Aerodynamic Models, in: *AIAA 40th Structures, Structural Dynamics, and Materials Conference,* St. Louis, Missouri, AIAA 99-1264-CP, April 1999, pp. 659–669.

[2] P. Beran, L. Huttsel and B. Buxton, Computational Aeroelasticity Techniques for Viscous Flow, in: *CEAS/AIAA/ICASE/NASA Langley International Forum on Aeroelasticity and Structural Dynamics,* Williamsburg, Virginia, June 1999.

[3] P.S. Beran and S.A. Morton, A Continuation Method for the Calculation of Airfoil Flutter Boundaries, *AIAA Journal of Guidance, Control, and Dynamics* **20**(1997), 1165–1171.

[4] E. Dowell, Eigenmode Analysis in Unsteady Aerodynamics: Reduced-Order Models, *AIAA Journal* **34** (1996), pp. 1578–1583.

[5] E. Dowell, K. Hall and M. Romanowski, Eigenmode Analysis in Unsteady Aerodynamics: Reduced-Order Models, *Appl. Mech. Rev.* **50** (1997), pp. 371–386.

[6] J. Edwards, Transonic Shock Oscillations and Wing Flutter Calculated with an Interactive Boundary Layer Coupling Method, NASA, TM-110284, 1996.

[7] R. Gordnier and R. Melville, Accuracy Issues for Transonic Wing Flutter Using 3-D Navier-Stokes, in: *AIAA 39th Structures, Structural Dynamics, and Materials Conference,* Long Beach, CA, AIAA-98-1729, April 1998.

[8] G. Guruswamy and E. Tu, Navier-Stokes Computations on Flexible Advanced Transport Wings in Transonic Regime, *Journal of Aircraft* **33** (1996), pp. 576–581.

[9] K. Hall, J. Thomas and E. Dowell, Reduced-Order Modelling of Unsteady Small-Disturbance Flows Using a Frequency-Domain Proper Orthogonal Decomposition Technique, in: *37th Aerospace Sciences Meeting*, AIAA 99-0655 January 1999.

[10] A. Harten, High Resolution Schemes for Hyperbolic Conservation Laws, *Journal of Computational Physics* **49** (1983), 357–393.

[11] P. Holmes, J.L. Lumley and G. Berkooz, Turbulence, Coherent Structures, Dynamical Systems and Symmetry, Cambridge University Press, 1996.

[12] A. Kurdila, C. Prazenica, O. Rediniotis and T. Strganac, Multiresolution Methods for Reduced Order Models for Dynamical Systems, in: *AIAA 40th Structures, Structural Dynamics, and Materials Conference,* St. Louis, Missouri, AIAA 99-1263-CP, April 1999, pp. 649–658.

[13] S.A. Mortara, J.C. Slater and P.S. Beran, A Proper Orthogonal Decomposition Technique for the Computation of Nonlinear Panel Response, in: *AIAA 41st Structures, Structural Dynamics, and Materials Conference,* Atlanta, GA, AIAA-2000-1936, April 2000.

[14] S.A. Morton and P.S. Beran, Hopf-Bifurcation Analysis of Airfoil Flutter at Transonic Speeds, *Journal of Aircraft* **36** (March–April 1999), 421–429.

[15] S.A. Morton, D. Rizzetta and R. Melville, Numerical Simulation of the Interaction Betwen a Leading-Edge Vortex and a Flexible Vertical Tail, in: *AIAA 39th Structures, Structural Dynamics, and Materials Conference,* Long Beach, CA, AIAA-98-1957, April 1998.

[16] H. Park and M. Lee, An Efficient Method of Solving the Navier-Stokes Equations for Flow Control, *International Journal of Numerical Methods* **41** (1998), 1133–1151.

[17] C.L. Pettit and P.S. Beran, Reduced-Order Modeling for Flutter Prediction, in: *AIAA 41st Structures, Structural Dynamics, and Materials Conference,* AIAA-2000-1446, Atlanta, GA, April 2000.

[18] O. Rediniotis, J. Ko, X. Yue and A. Kurdila, Synthetic Jets, Their Reduced Order Modeling and Applications to Flow Control, in: *37th Aerospace Sciences Meeting*, AIAA 99-0655, January 1999.

[19] M. Romanowski, Reduced Order Unsteady Aerodynamic and Aeroelastic Models Using Karhunen-Loève Eigenmodes, in: *AIAA/USAF/NASA/ISSMO Symposium on Multidisciplinary Analysis and Optimization,* (part 3), Bellvue, WA, AIAA 96-3981-CP, Sep. 1996, pp. 7–13.

[20] L.N. Sankar, S.Y. Ruo and J.B. Malone, Application of Surface Transpiration in Computational Aerodynamics, AIAA 86-0511, 1986.

[21] D. Schuster, J. Vadyak and E. Atta, Static Aeroelastic Analysis of Fighter Aircraft Using a Three-Dimensional Navier-Stokes Algorithm, *Journal of Aircraft* **27** (1990), 820–825.

[22] J.C. Slater, In-Situ Subspace Evaluation in Reduced-Order Modelling, Ball Aerospace, AFRL/VA Summer Faculty Fellowship Program, 2000.

[23] H. Yee, A Class of High-Resolution Explicit and Implicit Shock Capturing Methods, NASA, TM-101088, 1989.